Journal of Alloys and Compounds 509 (2011) 8987–8990

Contents lists available at ScienceDirect

Journal of Alloys and Compounds

journal homepage: www.elsevier.com/locate/jallcom

Formation and physical properties of a novel compound $Yb_3Pt_{23}Si_{11}$

D. Kaczorowski[a,*], A. Gribanov[b], S. Safronov[b], P. Rogl[c], Y. Seropegin[b]

[a] Institute of Low Temperature and Structure Research, Polish Academy of Sciences, P.O. Box 1410, 50-950 Wroclaw 2, Poland
[b] Chemistry Department, Moscow State University, Leninskie Gory, GSP-1, 119991 Moscow, Russia
[c] Institute of Physical Chemistry, University of Vienna, Währingerstrasse 42, A-1090 Wien, Austria

ARTICLE INFO

Article history:
Received 27 December 2010
Received in revised form 30 June 2011
Accepted 1 July 2011
Available online 12 July 2011

Keywords:
Ytterbium intermetallics
Crystal structure determination
Magnetic properties

ABSTRACT

The crystal structure of the novel compound $Yb_3Pt_{23}Si_{11}$ has been determined from powder X-ray diffraction data to be isotypic with cubic $Ce_3Pt_{23}Si_{11}$ (space group $Fm\bar{3}m$; $a = 1.68052(5)$ nm). Magnetic susceptibility, electrical resistivity and heat capacity measurements, performed down to 0.4 K, revealed that $Yb_3Pt_{23}Si_{11}$ is a moderately enhanced paramagnetic compound with fairly unstable 4*f* electronic shell.

1. Introduction

Since many years Ce, Yb, and U-based intemetallics have attracted much research interest owing to their intriguing physical properties such as valence fluctuations, Kondo-lattice behavior, heavy-fermion states, non-Fermi liquid features, unconventional superconductivity (see for instance [1,2]). Recently, in the course of our systematic study of the Yb–Pt–Si system, we identified a novel intermetallic compound $Yb_3Pt_{23}Si_{11}$. In this paper we report on the crystal structure of the new phase as well as on its magnetic, electrical and thermodynamic behavior at low temperatures. The structural and physical properties of $Yb_3Pt_{23}Si_{11}$ are compared with those of the related compounds: $La_3Pt_{23}Si_{11}$ [3], $Ce_3Pt_{23}Si_{11}$ [3–6], $Ce_3Pt_{23}Ge_{11}$ [7,8], and $U_3Pt_{23}Si_{11}$ [9,10].

2. Experimental details

A polycrystalline sample of $Yb_3Pt_{23}Si_{11}$ was prepared by melting the elements in an arc furnace on a water-cooled cooper hearth under purified argon atmosphere. Platinum and silicon were taken in stoichiometric amounts, while some excess (~3 mass%) of ytterbium was added due to highly volatile nature of this metal at high temperatures. The button was melted several times, and after each melting the weight losses were compensated by adding the appropriate amount of ytterbium metal (again with ~3 mass% excess). After the final melting, the weight of the sample was equal to that calculated for the ideal composition. No further heat treatment was applied.

The product was characterized by powder X-ray diffraction on a STOE STADI P transmission diffractometer equipped with a linear position sensitive detector. CuKα_1 radiation and Si external standard ($a_{Si} = 0.54307$ nm) were used. The lattice parameter was calculated using the STOE WinXPow program [11]. Structure refinement was performed using the Rietveld method implemented in the FULLPROF program [12,13]. Atom parameters were standardized with the aid of the program STRUCTURE TIDY [14].

Magnetic measurements were carried out in the temperature range 1.71–400 K and in magnetic fields up to 5 T using a Quantum Design MPMS-5 SQUID magnetometer. The electrical resistivity was measured over the range 4.2–300 K employing a conventional four-point dc technique and a home-made experimental setup. The heat capacity was studied from 6 K down to 0.4 K and in magnetic fields up to 5 T using a relaxation method implemented in a Quantum Design PPMS-7 platform.

3. Results and discussion

3.1. Crystal structure

The X-ray diffraction pattern of $Yb_3Pt_{23}Si_{11}$ (see Fig. 1) was properly described assuming a cubic structure of the $Ce_3Pt_{23}Si_{11}$ type (space group $Fm\bar{3}m$, $Z = 8$). The refined lattice parameter was $a = 1.68052(5)$ nm. The main crystallographic data are summarized in Table 1. Table 2 gives the atomic positions and the isotropic thermal displacement parameters, while Table 3 lists the shortest interatomic distances.

The unit cell of $Yb_3Pt_{23}Si_{11}$ is shown in Fig. 2. The Yb atoms, located at the 24*d* sites, are coordinated by tetragonal prisms build of eight Pt atoms. The Pt atoms occupy four inequivalent positions in the unit cell, whereas the Si atoms are distributed over three different sites. The refined crystal structure is fully ordered. For a detailed discussion of the crystallographic features in the $Ce_3Pt_{23}Si_{11}$ type structure, the interested reader is referred to Ref. [4].

$Yb_3Pt_{23}Si_{11}$ is a new representative of ternary compounds crystallizing with large face-centered cubic unit cells ($a \approx 1.7$ nm) such

* Corresponding author. Tel.: +48 71 34 350 21; fax: +48 71 34 410 19.
E-mail address: D.Kaczorowski@int.pan.wroc.pl (D. Kaczorowski).

0925-8388/$ – see front matter © 2011 Elsevier B.V. All rights reserved.
doi:10.1016/j.jallcom.2011.07.003

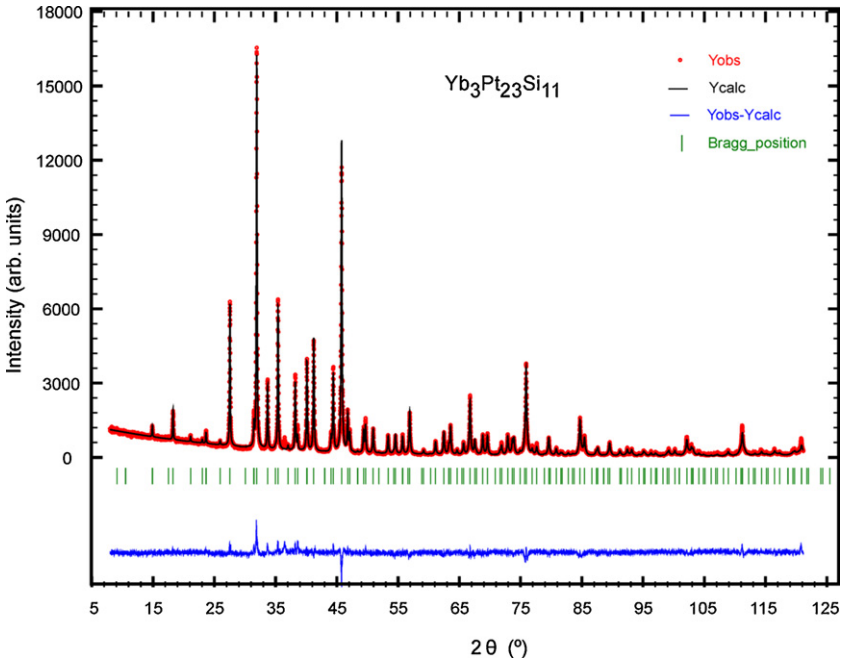

Fig. 1. X-ray diffraction pattern of $Yb_3Pt_{23}Si_{11}$ with the results of Rietveld refinement.

Table 1
Crystallographic details for $Yb_3Pt_{23}Si_{11}$.

Composition, EPMA (at.%)	$Yb_{8.4}Pt_{62.6}Si_{29.0}$
Composition from refinement (at.%)	$Yb_{8.1}Pt_{62.2}Si_{29.7}$
Formula from refinement	$Yb_3Pt_{23}Si_{11}$
Space group	$Fm\bar{3}m$ (No 225)
Pearson symbol	*cF296*
Structure type	$Ce_3Pt_{23}Si_{11}$
Lattice parameter (nm)	1.68052(5)
Two theta range (°)	8–121
Step (°)	0.01
Counting time per step (s)	90
Profile function	Pseudo-Voigt
Reflections measured	239
Number of variables	29
$R_F = \sum \lvert F_o - F_c \rvert / \sum F_o$	0.067
$R_I = \sum \left\lvert I_o - I_c \right\rvert / \sum I_o$	0.093
$R_{wP} = [\sum w_i \left\lvert y_{oi} - y_{ci} \right\rvert^2 / \sum w_i \lvert y_{oi} \rvert^2]^{1/2}$	0.119
$R_P = \sum \lvert y_{oi} - y_{ci} \rvert / \sum \lvert y_{oi} \rvert$	0.087
$R_e = [N - P + C / \sum w_i y_{oi}^2]^{1/2}$	0.045
$\chi^2 = (R_{wP}/R_e)^2$	7.0

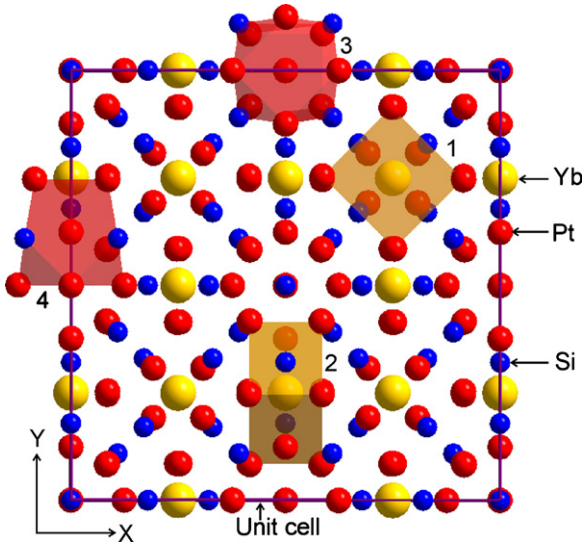

Fig. 2. Projection of the crystal structure of $Yb_3Pt_{23}Si_{11}$ onto the *XY* plane and coordination polyhedra of the Yb (1 and 2) and Pt_3 (3 and 4).

as the closely related compounds hitherto reported in the literature: $Ce_3Pt_{23}Ge_{11}$ [7,8], $Ce_3Pt_{23}Si_{11}$ [3–6], $La_3Pt_{23}Si_{11}$ [3], and $U_3Pt_{23}Si_{11}$ [9,10]. Whereas the crystal structure of $Ce_3Pt_{23}Ge_{11}$ was solved within space group $F\bar{4}3m$ (No. 216), all the other phases crystallize with space group $Fm\bar{3}m$ (No. 225) as for the present case of $Yb_3Pt_{23}Si_{11}$. It is worth mentioning that attempts to adopt for the latter compound the $Ce_3Pt_{23}Ge_{11}$ type structure (space group $F\bar{4}3m$) yielded significantly larger residual *R* values with markedly worse intensity fitting. Another remark to be made here is that despite $Ce_3Pt_{23}Si_{11}$ and $U_3Pt_{23}Si_{11}$ were reported in the literature as isotypic compounds with identical Wyckoff sequences, the two

Table 2
Atomic coordinates and isotropic thermal displacement parameters for $Yb_3Pt_{23}Si_{11}$.

Atom site	Wyckoff position	*x*/*a*	*y*/*b*	*z*/*c*	B_{iso} (10^2 nm^2)	Occupation
Yb	24*d*	0	1/4	1/4	0.83(4)	1.0
Pt_1	32*f*	0.08337(8)	0.08337(8)	0.08337(8)	0.89(1)	1.0
Pt_2	32*f*	0.30751(7)	0.30751(7)	0.30751(7)	0.89(1)	1.0
Pt_3	24*e*	0.3760(2)	0	0	0.89(1)	1.0
Pt_4	96*k*	0.08520(5)	0.08520(5)	0.25492(8)	0.89(1)	1.0
Si_1	24*e*	0.181(1)	0	0	1.7(1)	1.0
Si_2	32*f*	0.1697(5)	0.1697(5)	0.1697(5)	1.7(1)	1.0
Si_3	32*f*	0.3902(5)	0.3902(5)	0.3902(5)	1.7(1)	1.0

Table 3
Main interatomic distances in $Yb_3Pt_{23}Si_{11}$ (eds < 0.0005 nm).

Atom1	Multiplicity	Atom2	Distance (nm)
Yb	8×	Pt_4	0.3118
Pt_1	1×	Si_2	0.2513
	3×	Si_1	0.2567
	3×	Pt_1	0.2802
	3×	Pt_4	0.2883
Pt_2	3×	Si_2	0.2378
	1×	Si_3	0.2408
	3×	Pt_4	0.2698
	3×	Pt_2	0.2733
Pt_3	4×	Si_3	0.2619
	4×	Pt_4	0.2870
	4×	Pt_3	0.2948
Pt_4	1×	Si_3	0.2348
	1×	Si_1	0.2380
	1×	Si_2	0.2466
	1×	Pt_2	0.2698
	2×	Pt_4	0.2863
	1×	Pt_3	0.2870
	1×	Pt_1	0.2883
Si_1	4×	Pt_4	0.2380
	4×	Pt_1	0.2567
Si_2	3×	Pt_2	0.2378
	3×	Pt_4	0.2466
	1×	Pt_1	0.2513
Si_3	3×	Pt_4	0.2348
	1×	Pt_2	0.2408
	3×	Pt_3	0.2619

silicides seem to be occupation variants. While in $Ce_3Pt_{23}Si_{11}$, the sites 24*d* (0,1/4,1/4) and 24*e* (*x*,0,0) are occupied by Ce and Pt atoms [4], a reverse distribution of atoms was claimed for $U_3Pt_{23}Si_{11}$ [10]. Fig. 2 demonstrates differently oriented coordination polyhedra for atoms in the site 24*d* (0,1/4,1/4) (1 and 2) and for atoms in the site 24*e* (*x*,0,0) (3 and 4).

3.2. Physical properties

As shown in Fig. 3, the magnetic susceptibility of $Yb_3Pt_{23}Si_{11}$ is nearly temperature independent over an extended temperature range, yet rapidly increases below about 50 K. The observed behavior can be described in the entire temperature range in terms of the so-called modified Curie–Weiss

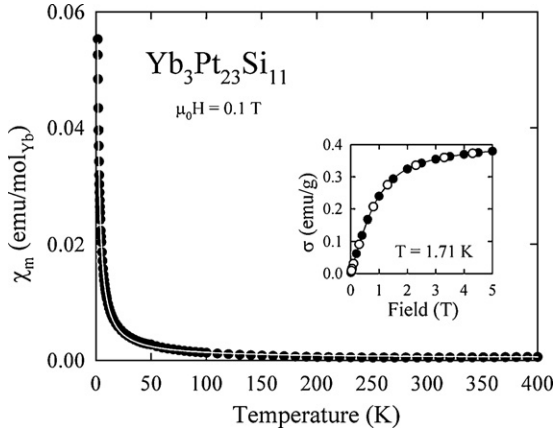

Fig. 3. Temperature dependence of the molar magnetic susceptibility of $Yb_3Pt_{23}Si_{11}$ measured in a field of 0.1 T. The solid line represents the least-squares fit discussed in the text. Inset: field variation of the magnetization in $Yb_3Pt_{23}Si_{11}$ measured at 1.71 K with increasing (full circles) and decreasing (open circles) magnetic field strength.

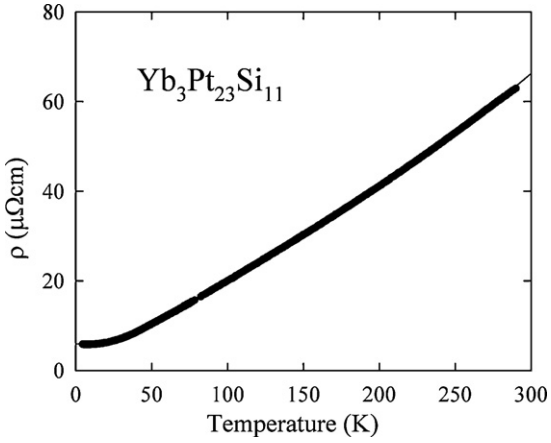

Fig. 4. Temperature dependence of the electrical resistivity of $Yb_3Pt_{23}Si_{11}$. The solid line represents the least-squares fit discussed in the text.

formula $\chi(T) = \chi_0 + C/T - \theta_p$, where χ_0 is a sum of temperature independent contributions, C is a Curie constant, and θ_p stands for the paramagnetic Curie temperature. The least-squares fit parameters are $\chi_0 = 3.42(4) \times 10^{-4}$ emu/(mol Yb-atom), $C = 0.1026(2)$ (emu K)/(mol Yb-atom) and $\theta_p = -0.2(2)$ K. The small value of the parameter C yields the effective magnetic moment of only 0.9 μ_B per Yb-atom, which is much smaller than the theoretical value calculated within the Russell-Saunders coupling scenario for a stable Yb^{3+} ions ($\mu_{eff} = 4.54\ \mu_B$). Frequently, Yb-based intermetallics form with divalent Yb ions that have nonmagnetic $4f^{14}$ electronic configuration. In such a case the intrinsic behavior of a given compound is represented by a Pauli-like term χ_0, while a Curie-like upturn in the magnetic susceptibility is attributed to magnetic impurities (usually some ytterbium oxides or/and hydroxides with Yb^{3+} ions, accumulated on grain boundaries). For the studied sample of $Yb_3Pt_{23}Si_{11}$ the latter scenario would imply the presence of as much as about 12% impurity atoms per formula unit. This very large amount of foreign phase can be ruled out based on the results of the X-ray diffraction. Therefore, the reduced value of μ_{eff} and the enhanced value of χ_0, derived from the $\chi(T)$ data, can be considered as fingerprints of unstable 4*f* shell in the compound studied. The strongly intermediate-valence (IV) character of $Yb_3Pt_{23}Si_{11}$ markedly contrasts with the Curie–Weiss paramagnetism of $Ce_3Pt_{23}Si_{11}$, occurring due to the presence of stable Ce^{3+} ions [3], which eventually give rise to a ferromagnetic phase transition at $T_C = 0.44$ K [6].

The non-magnetic IV nature of $Yb_3Pt_{23}Si_{11}$ is reflected also in the metallic-like temperature dependence of the electrical resistivity (see Fig. 4). The overall behavior of $\rho(T)$ can be represented by the function $\rho(T) = \rho_0 + 4RT(T/\Theta_R)^4 \int_0^{\Theta_R/T} (x^5 dx)/(e^x - 1)(1 - e^{-x}) + KT^3$, known as a Bloch–Grüneissen–Mott (BGM) formula [15]. In this expression, ρ_0 represents scattering the conduction electrons on static defects in the crystal lattice, the second term accounts for electron–phonon scattering processes (Θ_R is considered as a measure of the Debye temperature), whereas the T^3 term is due to *s–d* interband scattering. Fitting the BGM formula to the experimental data of $Yb_3Pt_{23}Si_{11}$ one obtains the parameters $\rho_0 = 5.9(1)\ \mu\Omega$ cm, $R = 0.166(5)\ \mu\Omega$ cm/K, $\Theta_R = 185(4)$ K, and $K = 4.25(2) \times 10^{-7}\ \mu\Omega$ cm/K^3. The small value of the residual resistivity, together with a relatively large residual resistivity ratio RRR ≈ 11 (RRR is the ratio of the resistivity measured at room temperature and ρ_0), indicates a fairly high quality of the polycrystalline sample measured. The derived value of Θ_R is remarkably smaller than the Debye temperature $\Theta_D = 266$ K, reported for the isostructural compound $La_3Pt_{23}Si_{11}$ (obtained from heat capacity data) [3]. This apparent discrepancy may be attributed to electronic

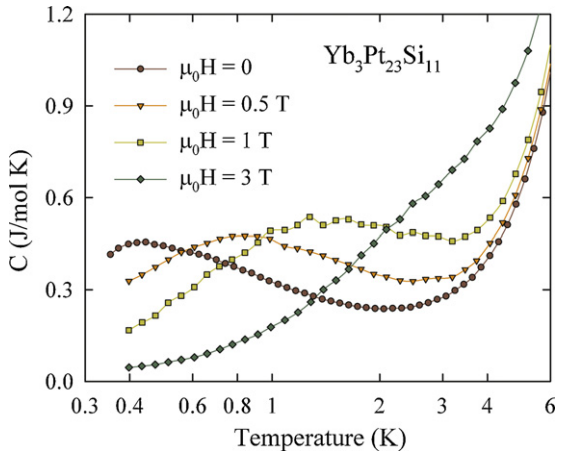

Fig. 5. Temperature dependencies of the low-temperature specific heat of $Yb_3Pt_{23}Si_{11}$ (note a logarithmic temperature scale) measured in a few different applied magnetic fields. The solid lines serve as a guide to the eye.

correlations, associated with the presumed valence fluctuations in $Yb_3Pt_{23}Si_{11}$ [16]. Worth noting is also the rather large value of K, directly related to the observed curvature in $\rho(T)$, that signifies the importance of scattering the conduction electrons via Mott-type processes.

The low-temperature specific heat data of $Yb_3Pt_{23}Si_{11}$ are displayed in Fig. 5. The most significant feature is a broad maximum in the $C(T)$ curve that forms below a minimum near 2 K. This behavior seems to correlate with the low-temperature tail in the magnetic susceptibility curve (compare Fig. 3), and hence it likely arises due to unstable 4*f* shell. Applying the afore-made rough estimate that the electronic ground state in $Yb_3Pt_{23}Si_{11}$ bears in its nature about 12% (per formula unit) of the $4f^{13}$ configuration, one may attempt to qualitatively interpret the maximum in $C(T)$ as a Kondo peak occurring in a system characterized by the total angular momentum $J = 7/2$. Indeed, the overall shape of the anomaly and the magnitude of the specific heat at the maximum agree reasonably well with the theoretical prediction [17]. Another indication of the Kondo nature of the maximum in $C(T)$ comes from its behavior in applied magnetic field: as may be inferred from Fig. 4, with increasing the field strength one observes a gradual shift of the maximum to higher temperatures with modest increase in its amplitude. The large Kondo contribution yields the enhanced specific heat at the lowest temperatures. Upon suppression of the maximum in $C(T)$ by applying a magnetic field of 3 T, the C/T ratio shows a clear tendency for saturation at temperatures $T \to 0$ (not shown) yielding the electronic Sommerfeld coefficient γ of about 110 mJ/(mol K^2). The latter value may be compared with $\gamma = 19$ mJ/(mol K^2) reported for the compound $La_3Pt_{23}Si_{11}$ [3]. This large difference in the electronic contribution to the heat capacity of the two nonmagnetic isostructural phases indicates prominent enhancement in the density of states at the Fermi level, being directly related to the unstable character of the 4*f* states in $Yb_3Pt_{23}Si_{11}$.

Acknowledgments

This work was supported by the Russian Foundation of Basic Research (project No. 11-03-01191-a) and the Austrian-Polish Scientific-Technical Exchange Program (project PL06/2009).

References

[1] H.R. Ott, Phys. B: Condens. Matter 378–380 (2006) 1–6.
[2] M. Brian Maple, R. Baumbach, N. Butch, J. Hamlin, M. Janoschek, J. Low Temp. Phys. 161 (2010) 4–54.
[3] D.C. Kundaliya, S.K. Malik, Phys. Rev. B 67 (2003) 1–3, 132411.
[4] A.I. Tursina, A.V. Gribanov, Y.D. Seropegin, K.V. Kuyukov, O.I. Bodak, J. Alloys Compd. 347 (2002) 121–123.
[5] A. Gribanov, A. Grytsiv, E. Royanian, P. Rogl, E. Bauer, G. Giester, Y. Seropegin, J. Solid State Chem. 181 (2008) 2964–2975.
[6] C. Opagiste, C. Paulsen, E. Lhotel, P. Rodière, R.M. Galera, P. Bordet, P. Lejay, J. Magn. Magn. Mater. 321 (2009) 613–618.
[7] A.V. Gribanov, Y.D. Seropegin, O.I. Bodak, V.V. Pavlyuk, L.G. Akselrud, V.N. Nikiforov, A.A. Velikhovski, J. Alloys Compd. 202 (1993) 133–136.
[8] R. Troc, D. Kaczorowski, T. Cichorek, B. Andraka, R. Pietri, Y.D. Seropegin, A.V. Gribanov, J. Alloys Compd. 262–263 (1997) 211–214.
[9] C. Geibel, C. Kämmerer, E. Göring, R. Moog, G. Sparn, R. Henseleit, G. Cordier, S. Horn, F. Steglich, J. Magn. Magn. Mater. 90–91 (1990) 435–437.
[10] J.N. Chotard, O. Tougait, H. Noël, P. Rogl, A. Zelinskiy, O.I. Bodak, J. Alloys Compd. 407 (2006) 36–43.
[11] STOE WINXPOW (Version 1.06), Stoe & Cie GmbH, Darmstadt, Germany, 1999.
[12] J. Rodriguez-Carvajal, Satellite Meeting on Powder Diffraction of the XV Congress of the IUCr, Book of Abstracts, Toulouse, France, 1990, p. 127.
[13] T. Roisnel, J. Rodriguez-Carvajal, in: Proceedings of the European Powder Diffraction Conference (EPDIC7), Mater. Sci. Forum, Book of Abstracts, 2000, p. 118.
[14] E. Parthé, L. Gelato, B. Chabot, M. Penzo, K. Cenzual, R. Gladyshevskii, TYPIX Standardized Data and Crystal Chemical Characterization of Inorganic Structure Types , Springer-Verlag, Berlin, Heidelberg, 1994.
[15] N.F. Mott, H. Jones, The Theory of the Properties of Metals and Alloys , Oxford University Press, 1958.
[16] M. Giovannini, H. Michor, E. Bauer, G. Hilscher, P. Rogl, R. Ferro, J. Alloys Compd. 280 (1998) 26–38.
[17] V.T. Rajan, Phys. Rev. Lett. 51 (1983) 308–311.